International Journal of Nanomedicine

Dovepress
Taylor & Francis Group

Open Access Full Text Article

ORIGINAL RESEARCH

Enhanced Antitumor Immunity Through T Cell Activation with Optimized Tandem Double-OX40L mRNAs

Zhuoya Deng[1–3,*], Yuying Tian[1,*], Jing Wang[1], Yongru Xu[1], Zherui Liu[3,4], Zhaohui Xiao[1], Zhaohai Wang[1], Minggen Hu[1], Rong Liu[1], Penghui Yang[1]

[1]Faculty of Hepato-Pancreato-Biliary Surgery, Institute of Hepatobiliary Surgery, the First Medical Center, Chinese PLA General Hospital, Beijing, People's Republic of China; [2]Beijing Youan Hospital, Capital Medical University, Beijing, People's Republic of China; [3]The Fifth Medical Center, Chinese PLA General Hospital, Beijing, People's Republic of China; [4]Peking University 302 Clinical Medical School, Peking University, Beijing, People's Republic of China

*These authors contributed equally to this work

Correspondence: Penghui Yang; Rong Liu, Email ypenghuiamms@hotmail.com; liurong301@126.com

Purpose: The tumor immune microenvironment (TIME) is often dysfunctional and complex, contributing to tumor metastasis and drug resistance. This study investigates the use of mRNA-based cancer agents as promising tools to combat and reverse refractory TIME conditions.

Methods: We optimized and engineered an mRNA cancer agent encoding double tandemly repeated sequences of the T cell costimulator Oxford 40 ligand (diOX40L). The diOX40L mRNAs were encapsulated into lipid nanoparticles (LNPs) for effective delivery. The research explored its safety and antitumor effects through a series of in vivo and in vivo experiments.

Results: Our results demonstrate that diOX40L mRNAs efficiently express increased levels of OX40L proteins. The optimized diOX40L mRNA cancer agent generated potent immune costimulatory signals within the TIME, leading to decreased tumor growth and improved survival compared to the original sequence agent. OX40L expression in subcutaneous tumors promoted $CD4^+$ and $CD8^+$ T cell activation, resulting in heightened IFN-γ and IL-2 secretion and robust immune responses. Combination therapy involving PD-1 antibodies and diOX40L substantially enhanced antitumor efficacy, with increased infiltration of activated $CD4^+$ and $CD8^+$ T cells.

Discussion: In conclusion, our findings highlight the therapeutic potential of the optimized diOX40L mRNA cancer agent in cancer treatment and its potential as an innovative alternative to protein-based therapies. The study underscores the significance of mRNA-based agents in modulating the immune microenvironment and enhancing antitumor responses.

Keywords: tumor immunotherapy, tumor immune microenvironment, OX40L mRNA, malignant tumor, lipid nanoparticles

Introduction

Cancer poses a substantial threat to human health, characterized by its high morbidity and mortality rates. Among cancer types, hepatocellular carcinoma (HCC) has emerged as the fourth leading cause of cancer-related mortality.[1] Conventionally, HCC therapy has mainly relied on surgical treatment, adjuvant radiotherapy, and chemotherapy. However, these modalities have limited therapeutic effects against advanced HCC.[2] Immunotherapy such as immune checkpoint inhibitors has revolutionized cancer therapeutic management, becoming a highly effective cancer treatment.[3] The use of immunotherapy in HCC following the success of a Phase II trial of anti-PD1 therapy (nivolumab).[4]

The presence of suppressive and intricately organized immunocyte infiltration within the tumor microenvironment (TME) is a well-known contributor to tumor metastasis and drug resistance.[5,6] To improve the sensitivity of immunotherapy and overcome drug resistance, it is crucial to investigate and understand the intricacies of the dysfunctional TME.[7,8] Recently, cancer patients are benefiting from immunoactivated tumor microenvironment with ICIs.[9] However, there are still controversies and differences in choosing ICIs as the best first-line treatment.[10,11] Preclinically, increasing

Received: 9 July 2024
Accepted: 5 November 2024
Published: 19 March 2025

© 2025 Deng et al. This work is published and licensed by Dove Medical Press Limited. The full terms of this license are available at https://www.dovepress.com/terms.php and incorporate the Creative Commons Attribution – Non Commercial (unported, v3.0) License (http://creativecommons.org/licenses/by-nc/3.0/). By accessing the work you hereby accept the Terms. Non-commercial uses of the work are permitted without any further permission from Dove Medical Press Limited, provided the work is properly attributed. For permission for commercial use of this work, please see paragraphs 4.2 and 5 of our Terms (https://www.dovepress.com/terms.php).

the expression of costimulatory molecules is a promising candidate for the next generation to enhance immunotherapy.[12–14] Members of the tumor necrosis factor receptor/tumor necrosis factor superfamily, OX40 (CD134) and OX40L (CD252) are expressed on activated $CD4^+$ and $CD8^+$ T cells as well as on a variety of other lymphoid and non-lymphoid cells. In line with the modulatory functions that targeted T cells, OX40-OX40L interactions have been found to play a role in multiple TIME cell infiltration, making them attractive candidates for intervention in the clinic.[15] It was discovered that the OX40-OX40L pathway could contribute to enhanced responses in a tumor model using OX40L fusion proteins and anti-OX40 mAbs.[16,17] Following several agonist drugs targeting OX40 and immunostimulants expressing OX40L have been developed as adjuvant immunotherapy for cancers.[18] Thus, modulating the OX40-OX40L axis, particularly by activating OX40 on T cells, represents an effective strategy to enhance overall curative outcomes.[19]

Conventional protein-based platforms for producing OX40-OX40L agonists or immunostimulants often encounter manufacturing-related difficulties, including tendencies to aggregate over time, the presence of inherent production process impurities, and inherent drug product properties.[20] These challenges result in costly, time-consuming, and labor-intensive manufacturing processes. Therefore, there is a pressing need to explore alternative protein expression platforms. mRNA cancer agents have emerged as a promising platform for cancer immunotherapy due to their high efficacy, safe administration, rapid development potential, and cost-effective manufacturing.[21] This mRNA-based protein platform is synthesized by in vitro transcription of mRNA and encapsulating with LNP. Then the thoroughly purified agent was injected to complete the delivery of mRNA and the expression of protein.[22] Thus, mRNA cancer agents are being swiftly adopted for targeting a range of elements, including tumor-associated antigens, neoantigens, antibodies, and immunostimulants, achieved through sequence screening and optimization. For example, the pioneer player Moderna has developed two mRNA products about OX40L for intratumoral immunostimulatory activities. Phase I clinical trials are now being conducted to assess their safety and tolerability when administered repeatedly. One drug is mRNA-2416, which treats metastatic ovarian cancer and lymphoma by utilizing mRNA encoding OX40L either alone or in combination with the PD-L1 inhibitor durvalumab (NCT03323398).[23] The other, called mRNA-2752, is intended to treat lymphoma and is made up of the mRNAs OX40L/IL-23/IL-36 (NCT03739931).[24,25] Meanwhile, the OX40L mRNA cancer agent has been reported in our previous articles, demonstrating its therapeutic potential.[26,27] For the purposes of this investigation, we have undertaken additional sequence optimization to investigate broader potential and mechanisms of immunostimulants.

In this study, we engineered a double-OX40L mRNA cancer agent to achieve a substantial increase in OX40L protein expression. Through intratumoral administration, we observed a heightened release of OX40L into the tumor microenvironment (TEM) in vivo. The therapeutic potential of the diOX40L mRNA agent was evaluated using an H22 tumor model, where it demonstrated remarkable efficacy and significantly prolonged the survival of H22-bearing mice. Similar promising results were obtained in the B16F10 mouse melanoma model. These findings suggest the feasibility of utilizing engineered OX40L mRNA agents as part of immunotherapy for liver cancer. Moreover, the mRNA agent's capacity to express optimized proteins with locoregional delivery offers a promising and non-toxic approach to enhance cancer immunotherapy.

Materials and Methods

Sequence Optimization of diOX40L mRNA and mRNA Preparation

First designing the template for constructing mRNA, we inserted the transcription template into plasmid pcDNA3.1 through the restriction site. In this way, the cDNA sequence containing the 5′ end, ORF, and 3′ end was built on plasmid pcDNA3.1. The selection restriction sites are BamH I and Xba I through software DNAMAN design. The sequence of ORF consists of two OX40L concatenated by linker. The recombinant pcDNA3.1 plasmid encoding diOX40L was synthesized by Biotech Bioengineering (Shanghai) Co. and confirmed by DNA sequencing. The plasmid with the target fragment was extracted and the linearized template diOX40L-pcDNA3.1 was obtained by mono-enzymatic cleavage of the target plasmid by Xba I in a water bath at 37°C for 30 min, followed by column purification using a DNA purification kit. Agarose gel electrophoresis and nucleic acid concentration detection were performed to evaluate the quality of the

plasmid. The mRNA was produced in vitro by T7 RNA polymerase-mediated transcription (Novoprotein, GMP-E121) from the linearized DNA template from plasmids. 5′-triphosphate (UTP) substituted with N1-methylpseudo-UTP Stable diOX40L mRNA was produced by using cowpox cap system to synthesize Cap1 structures and using *Escherichia* coli poly(A) polymerase to add poly(A) tails of >100 bases. The mRNA was purified by RNA purification kit (NEB, T2040) and the quality of mRNA was evaluated by performing agarose gel electrophoresis and nucleic acid concentration assay.

LNP Formulation

The final mRNA-diOX40L-LNP formulations were prepared using the method previously described.[24] The LNP formulations are composed of Dlin-MC3-DMA, DSPC, Cholesterol and DSPE-PEG2000 (molar ratio at 50:10:38.5:1.5). The after-encapsulated diOX40L mRNAs were collected by ultracentrifugation and characterized using DLS for quality control. The particle size was assayed by using electron microscopy.

Patients Characterization and Sample Collection

A total of 29 paired HCC tissues and paracancerous tissues were collected from patients at the Fifth Medical Center of Chinese PLA General Hospital. The tissue specimens collected from each subjects were stored at −80°C. All of these patients were identified with primary HCC by pathological diagnosis. The study complies with the *Declaration of Helsinki* and was approved by the Ethics Committee of the Fifth Medical Center of Chinese PLA General Hospital. All patients provided written informed consent.

Real-Time Quantitative PCR

Total RNA of HCC and paracancerous tissues collected from HCC patients was extracted according to manufacturer's instructions of R1200 RNA Isolation Kit (Solarbio, Beijing, China). cDNA was synthesized based on the instructions of cDNA Synthesis Mix Kit (KR118, Tiangen, Beijing, China). An SYBR Green qPCR PreMix (FP207, Tiangen, Beijing, China) was applied for the quantification of mRNA. GAPDH level was used for the normalization of OX40L expression. Relevant sequences used were listed in Supplementary Table S1. The data were analyzed using the $2^{-\Delta\Delta ct}$ method.

Cell Culture and Strains

Human endothelial kidney cell line HEK293T, mouse HCC cell lines H22 and mouse melanoma cell lines B16F10 were obtained from ATCC. HEK293T and H22 cells were grown in Dulbecco's modified Eagle's medium (DMEM). B16F10 cells were grown in minimum essential medium (MEM). All culture mediums were supplemented with 10% fetal bovine serum and 1% penicillin-streptomycin. Competent cells DH5α were purchased from Tiangen for plasmid amplification.

In vitro Transfection of mRNA-diOX40L-LNP

HEK293T cells were seeded in 6-well plates at 5×10^5 cells/well. Twenty-four hours later, the OX40L-mRNA (prepared by method previously described[24]) and diOX40L-mRNA were transfected by LNP. Cells were collected at 24, 48 and 72 hours after transfection and analyzed by Western blotting and immunofluorescent as described below.

Western Blotting Assay

Cells from control, OX40L and diOX40L group were harvested at 24, 48 and 72 hours after transfection using 0.25% EDTA-Trypsin. Total protein was extracted using RIPA buffer (Solarbio, R0010). Protein concentrations were determined using a BCA Protein Assay Kit according to the manufacturer's instructions. Next, proteins (10μg per lane) were resolved on 10% SDS-PAGE. For immunoblotting, proteins were transferred to a polyvinylidene difluoride membrane. Blots were incubated for 1 hour at room temperature in blocking buffer containing 5% bovine serum albumin (BSA; Solarbio, SW3015); incubated overnight at 4°C with rabbit anti-OX40L antibody (1:1500 dilution, CST, 14991) and mouse anti-β-actin antibody (1:1500 dilution, CST, 3700); and subsequently incubated with HRP-conjugated goat anti-rabbit (1:5000 dilution) and HRP-conjugated goat anti-mouse (1:5000 dilution) antibodies for 1.5 h at room temperature. The blots were visualized using an ECL detection system.

Immunofluorescent Assay

For the immunofluorescent examination, 1×10^5 HEK293T cells were seeded on glass coverslips in 12-well plates pretreated with TC (Solarbio). After incubation for 24 h to reach 75% confluence, the cells were transfected with diOX40L mRNA and incubated at 37°C for 60 min. Then, the mixture was removed, and 1.5 mL fresh medium was added to the transfected cells. After further incubation at 37°C for 24 h, the wells were fixed with 4% paraformaldehyde for 30 min followed by three washes with PBST. Cells were incubated in a blocking buffer containing 5% BSA. Next, cells were incubated with primary antibodies against rabbit anti-OX40L antibody (1:200, Abcam, ab263910) in PBST at 4 overnight. The coverslips were washed three times with PBST and incubated with Alexa Fluor® 488-conjugated goat anti-rabbit IgG H&L (1:250, Abcam, ab150077) for 1 h at room temperature. Nuclei were counterstained with DAPI (Solarbio, C0065). Images were taken with a confocal laser scanning microscope.

In vivo HCC Mouse Model

All animal experiments were approved by the Animal Welfare and Ethics Committee of the Chinese PLA General Hospital in accordance with the *Regulations on the Administration of Laboratory Animals* and the relevant internationally recognized animal welfare guidelines (*Guide for the Care and Use of Laboratory Animals*) to ensure that the animals received proper care and humane treatment throughout the experimental process. Four- to six-week-old female BALB/C mice were purchased from SPF (Beijing) Biotechnology Co. All mice were provided with food and water ad libitum and maintained in a 12-h light–dark cycle under standard conditions at SPF environment. For subcutaneous experiments, H22 cells were pre-inoculated intraperitoneally into Kunming mice. One week later, cells with ascites were harvested and 5×10^6 H22 cells were subcutaneously injected into the left flank of the mice. When the tumor volume reached to $100mm^3$, the mice were randomly divided into three groups (n=6/group). mRNA-OX40L-LNP or mRNA-diOX40L-LNP or LNP was intratumorally administrated at 11.5 μg into mice in each group, respectively. Intratumoral injections were performed six times at 3-day intervals.

As to subcutaneous experiments of diOX40L-mRNA combined PD-1, four- to six-week-old female BALB/C mice and H22 cells were also used as described above. 5×10^6 H22 cells were subcutaneously injected into the left flank of the mice and when the tumor volume grew to 100 mm^3, the mice were randomly divided into four groups (n=6/group). LNP was intratumorally administrated six times at 3-day intervals at 11.5 μg into negative control (NC) group. mRNA-diOX40L-LNP was intratumorally administrated six times at 3-day intervals at 11.5 μg into diOX40L group and diOX40L+PD-1 group. PD-1 antibody was intraperitoneal injected two times a week for two weeks at 10mg/kg into diOX40L+PD-1 group and PD-1 group.

All experiments continuously measured tumor volume and survival condition. The endpoints of the study were animal death or a tumor reaching 2000 mm^3. Tumors were collected and weighed, tumor volume was calculated as (tumor length × tumor $width^2\times0.5$), Kaplan–Meier survival curves were plotted after 21 days.

In vivo Melanoma Mouse Model

Four- to six-week-old female C57BL/6 mice were purchased from SPF (Beijing) Biotechnology Co. and housed in an SPF environment with regular watering and feeding. For melanoma mouse model, 5×10^5 B16F10 cells were subcutaneously injected into the left flank of the mice. When the tumor volume reached to $100mm^3$, the mice were randomly divided into four groups (n=8/group). NC group was intratumorally administrated at 11.5 μg LNP four times at 3-day intervals. diOX40L group was intratumorally administrated at 11.5 μg mRNA-OX40L-LNP four times at 3-day intervals. diOX40L+PD-1 group was intratumorally administrated at 11.5 μg mRNA-OX40L-LNP four times at 3-day intervals and was intraperitoneal injected PD-1 antibody two times a week for one week at 10mg/kg. PD-1 group was intraperitoneal injected PD-1 antibody two times a week for one week at 10mg/kg. Subcutaneous experiments continuously measured tumor volume and survival condition. The endpoints of the study were animal death or a tumor reaching 2000 mm^3. Tumors were collected and weighted, and tumor volume was calculated as (tumor length × tumor $width^2\times0.5$). Tumor draining lymph node (TdLN) was collected. The orbital blood was collected and centrifuged at 3000×g at 4°C for 15 min, serum was collected and stored at −80°C for further test. Kaplan–Meier survival curves were plotted after 21 days.

Flow Cytometry Assay

The evaluation of immune cells population was performed by using flow cytometry assay. The mouse tumor single-cell suspension was acquired through grinding and percoll gradient separation. Then, cells were activated by cell activation cocktail with Brefeldin A (Biolegend). Cells were stained with the anti-CD45-Alex Fluor 700 antibody, anti-CD3-DsRed antibody, anti-CD4-PE-Texas Red-A antibody, anti-CD8-Percp-Cy5.5 antibody, anti-Ly6G-APC/cyanine7 antibody, anti-CD44-PE/cyanine7 antibody, anti-CD25-PE/cyanine5 antibody, anti-CD11b-Brilliant Violet 711 antibody, anti-B220-Qdot 605 antibody, anti-CD62L-FITC, anti-CTLA-4-APC. Extracellular staining was fixed with cell fixation fluid, after which intracellular staining was performed. Intracellular antibodies were diluted in Intracellular Staining Permeabilization Wash buffer (Biolegend, 421002). Intracellular staining was anti-Granzyme B-DAPI antibody. For the experiment of aPD-1 combined with diOX40L mRNA, the procession of tumor single-cell suspension was same as above. The TDLN single-cell suspension was screened by grinding through the cell sieve. Anti-CD45-APC/cyanine7 antibody, anti-CD3-PE/cyanine7 antibody, anti-CD4-FITC antibody, anti-CD8-Percp-Cy5.5 antibody, anti-CD69-PE antibody, anti-CD44-Brilliant Violet 510 antibody, anti-CD62L-Alex Fluor 700 antibody, anti-IFNγ-APC antibody and anti-IL2-Brilliant Violet 421 antibody were used to evaluate the T cells subpopulation. All of the stained antibodies were purchased at Biolegend. Finally, the cells were washed three times with PBS and analyzed using FACS.

In vivo Systemic Toxicities Evaluation

To assess the potential for liver and renal toxicity of mRNA-diOX40L-LNP, serum samples were obtained from a subcutaneous melanoma mouse model. Alanine aminotransferase (ALT), aspartate aminotransferase (AST), and creatine kinase (CK) in serums were measured enzymatically using the Alanine aminotransferase Assay Kit (C009-2-1, Nanjing Jiancheng Bioengineering Institute), Aspartate aminotransferase Assay Kit (C010-2-1, Nanjing Jiancheng Bioengineering Institute), and Creatine kinase assay kit (A032-1-1, Nanjing Jiancheng Bioengineering Institute) according to the manufacturer's instructions, respectively.

Statistical Analysis

Statistical analysis was performed using GraphPad Prism software. Data are expressed as medians ± minimum to maximum or means ± SDs. Fisher's exact test and *t*-test were used for comparisons between the two groups. Multiple comparisons were performed using one-way ANOVA with Dunnett's multiple comparison post hoc test while in survival test, the statistical significance was analyzed by Wilcoxon log-rank. A P value < 0.05 was considered statistically significant ($^{*}P < 0.05$; $^{**}P < 0.01$; $^{***}P < 0.001$).

Results

Preparation and Characterization of the Optimized diOX40L mRNA Cancer Agent

As shown in Figure 1A, the opening reading frame (ORF) of the diOX40L mRNA, which is the protein-coding sequence region, is composed of double OX40L sequences linked by linker ligation. In addition, intact mRNA molecule includes 5′ UTR and 3′ UTR to regulate the translation of the mRNA; the 2′-O-methylated Cap0 (Cap1) to imitate the natural cap structure to help the ribosome recognition; and Poly(A) tail to protect mRNA from its degradation. At the same time, the Kozak sequence was selected in 5′ UTR region to mediate the initiation of protein translation. Based on the RNA secondary structure prediction algorithm combined with bioinformatics analysis, the OX40L with tandem structure is the target sequence to enhance the molecular biological structure. Finally, we determined the mRNA sequence with the most stably expressed diOX40L. In the subsequent experiments, for the studies on mice, we used the mouse-derived OX40L sequence. In the in vitro experiments, we utilized the human-derived sequence for validation. The optimization results of human-derived sequence were provided in the Supplementary Table S2.

The entire coding sequence was constructed on a plasmid vector pcDNA3.1 (+), gel electrophoresis of which showed in Figure 1B. The *Xba I*-digested recombinant plasmid allowed the polymerase to perform conventional in vitro transcription. The linearized plasmid size was about 6600 bp (Figure 1C). The gel electrophoresis of diOX40L mRNA shows demonstrating that the length of the mRNA fits with the diOX40L (Figure 1C). For successful protein expression,

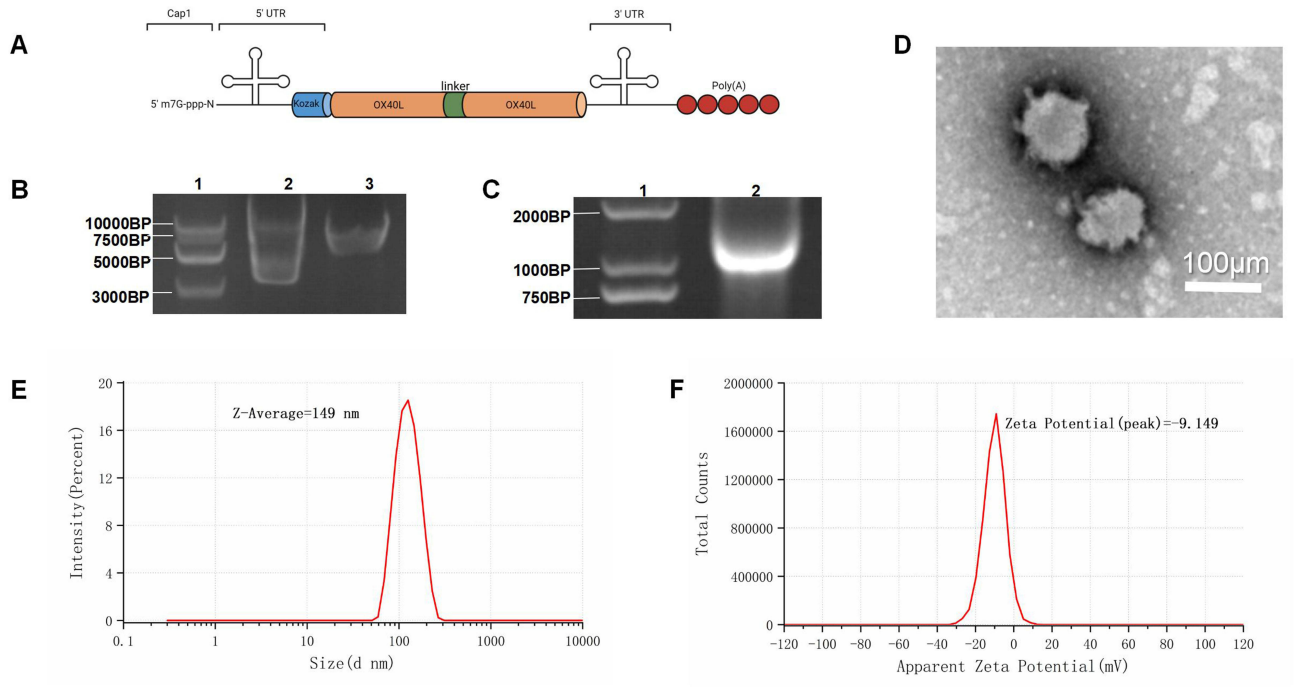

Figure 1 Optimization and characterization of encapsulated diOX40L mRNA agent. **(A)** Design of an optimized diOX40L mRNA. (**B)** Identification of recombinant plasmid and restriction-digested plasmid by gel electrophoresis. 1) 15000 bp marker, 2) diOX40LpcDNA3.1 and 3) *Xba I*-digested diOX40L-pcDNA3.1. (**C)** Electrophoretic profile of mRNA 1) 2000 bp marker; 2) diOX40L mRNA. (**D)** TEM image of LNP-formulated diOX40L mRNA. Scale bar, 100 nm. (**E)** Size distribution of LNP-formulated diOX40L mRNA. (**F)** ζ potential of LNP-formulated diOX40L mRNA.

we prepared LNP delivery formulations to carrier the mRNA into the cells. Transmission electron microscope (TEM) observation and dynamic light scattering (DLS) analysis revealed that the LNP encapsulated diOX40L mRNA exhibited regular spherical membrane structures with average diameters of about 100 nm (Figure 1D-F).

More Efficient Expression of Immunostimulant OX40L in vitro and in vivo

We detected the mRNA expression level of OX40L in HCC tissues and paracancerous tissues by RT-qPCR and demonstrated that the expression of OX40L exists in HCC and the expression level is higher than that in adjacent tissues (Figure 2A). Then, we evaluated the delivery efficiency of LNP and the capacity of diOX40L mRNA-based protein expression. To this end, the transfection study was performed in the HEK293T cells in vitro. We compared the expression of OX40L between the optimized diOX40L mRNA and the original single OX40L mRNA by Western blot. The results showed a higher expression level of OX40L using diOX40L mRNA agents (Figure 2B). We performed a time-dependent experiment to detect the expression of OX40L protein and proved that the protein expression was the highest at 24 h (Figure 2C). According to laser confocal microscope analysis of transfected HEK293T cells, as shown in Figure 2D, the cellular distribution of OX40L was on the cell surface and the expression reduced with time, in agreement with the findings in Figure 2C.

To explore whether OX40L is well expressed in vivo, we injected diOX40L mRNA, original single OX40L mRNA, and non-coding sequence preparations, respectively, into subcutaneous tumor. After 24 hours intratumorally injection of 10μg mRNA preparations, we collected the tumor tissue and performed flow cytometry analysis to verify the expression of OX40L in vivo and the feasibility of the LNP formulation (Figure 2E). All analyzed H22 cancer cells expressed OX40L higher in the group of diOX40L than the other two groups, by percentage and Mean fluorescence intensity (MFI) (Figure 2F-G).

Comparison of Antitumor Effect of the diOX40L mRNA versus Original OX40L mRNA

To evaluate the efficacy of diOX40L mRNA for the in vivo treatment of liver tumors, we utilized the H22 subcutaneous tumor-bearing mouse model. At the same time, to better evaluate the effect of the agents on the larger H22 tumors, we

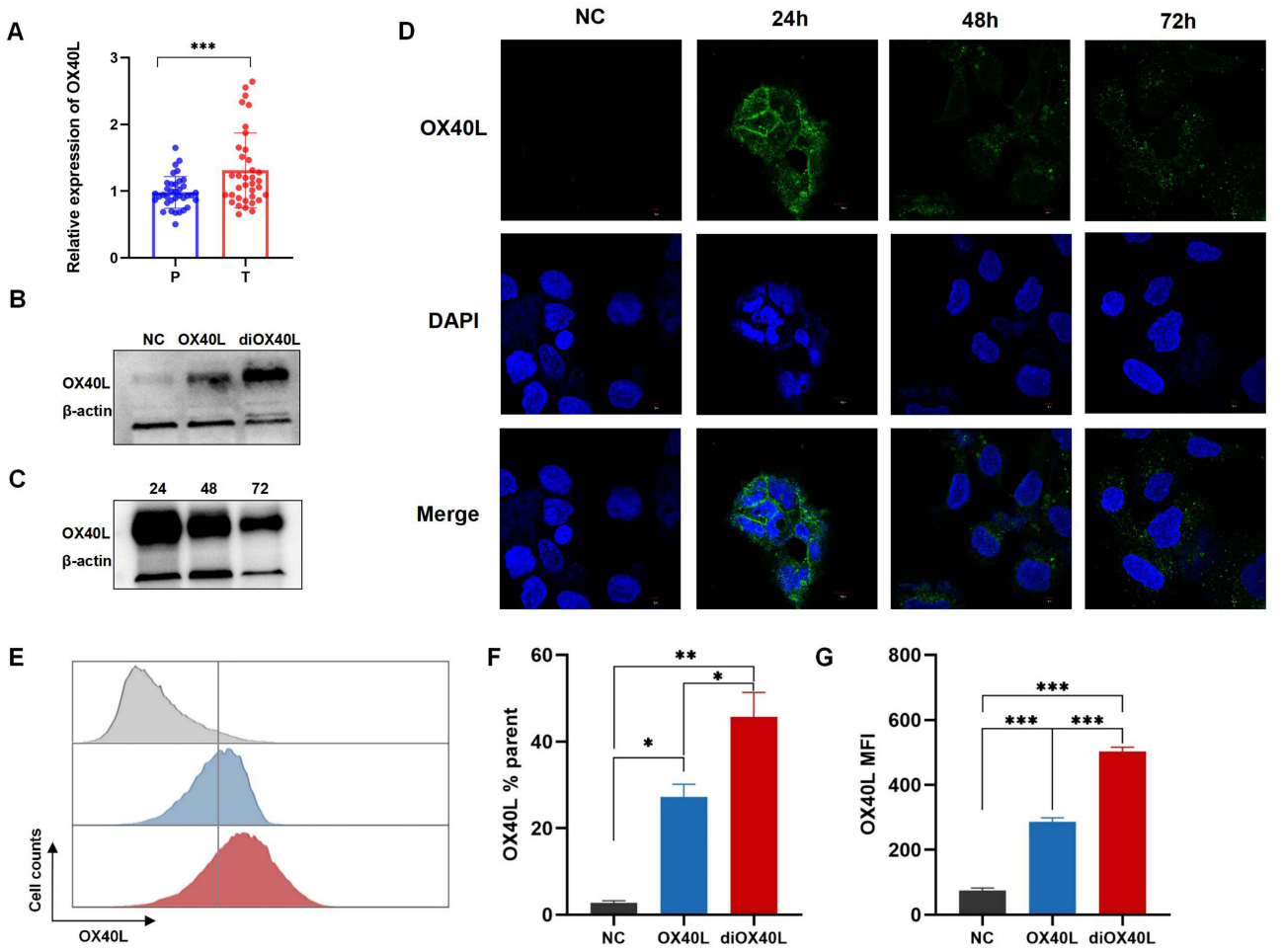

Figure 2 In vitro transfection of the diOX40L mRNA. **(A)** Reverse transcription (RT) quantitative (q)PCR assay of OX40L expression on patient-derived HCC. Data were processed using GraphPad Prism 8 and are presented as the mean ± SD. The *P* values were determined using a *t*-test. ***, $P < 0.001$. **(B)** Western blot analysis of OX40L expression in HEK293T cells after the indicated treatments for 24 hours. **(C)** Western blot analysis of OX40L expression in HEK293T cells after the diOX40L mRNA transfected for 24, 48, and 72 hours. **(D)** Immunofluorescence imaging of OX40L expression in HEK293T cells treated with noncoding and diOX40L mRNA for 24 hours, 48 hours, and 72 hours. OX40L protein was stained in green, and DAPI in blue. **(E)** Flow cytometry analysis of cell uptake efficiency by H22 subcutaneous tumors after intratumoral injection with different mRNA agents. **(F)** The percentages were used to present the flow cytometry data. **(G)** The mean fluorescence intensity (MFI) was used to present the flow cytometry data. Data of **(E, F)** were processed using GraphPad Prism 8 and are presented as the mean ± SD. The *P* values were analyzed by One-way ANOVA with multiple comparisons. *, $P < 0.1$; **, $P < 0.01$; ***, $P < 0.001$.

delayed the starting point of the treatment from 80 mm^3 to 100 mm^3 of the tumor volume, which was different from the previous article. Twelve days after tumor implantation, animals received intratumorally injection with diOX40L and original OX40L and non-coding mRNA preparation at the dose of 10μg per mouse.[26] Experiment schedule is shown in Figure 3A. Tumor progression was monitored by measuring its volume at two-day intervals. When the tumor volume exceeded 1500 mm^3, the animal was considered dead. Original OX40L and diOX40L agents all slowed H22 progression and the diOX40L agents were effective than others in inhibiting the growth of H22 tumors in vivo (Figure 3B-C). Moreover, prolonged median survival of 33 days after the H22 cells inoculation was shown among the three groups (Figure 3D). The volume and weight of the tumors isolated on day 21 are shown in Figure 3E. Photographs of isolated H22 tumors are shown in Figure 3F. To further explore the antitumor mechanisms of the diOX40L mRNA in HCC, we extracted lymphocytes from the tumor tissues and detected the phenotypes of immune cells by using flow cytometry. Our results showed that the cytotoxic T cells, helper T cells, naive T cells, central memory T cells and effector T cells were more abundant in the diOX40L group than both the OX40L group and control group. Compared with the control group, the diOX40L group was more overrepresented on neutrophils, B cells, and $GrzmB^+$ T cells. However, Treg cells in diOX40L group did not show significant differences from the other two groups (Figure 3G). Based on the above animal

https://doi.org/10.2147/IJN.S479434

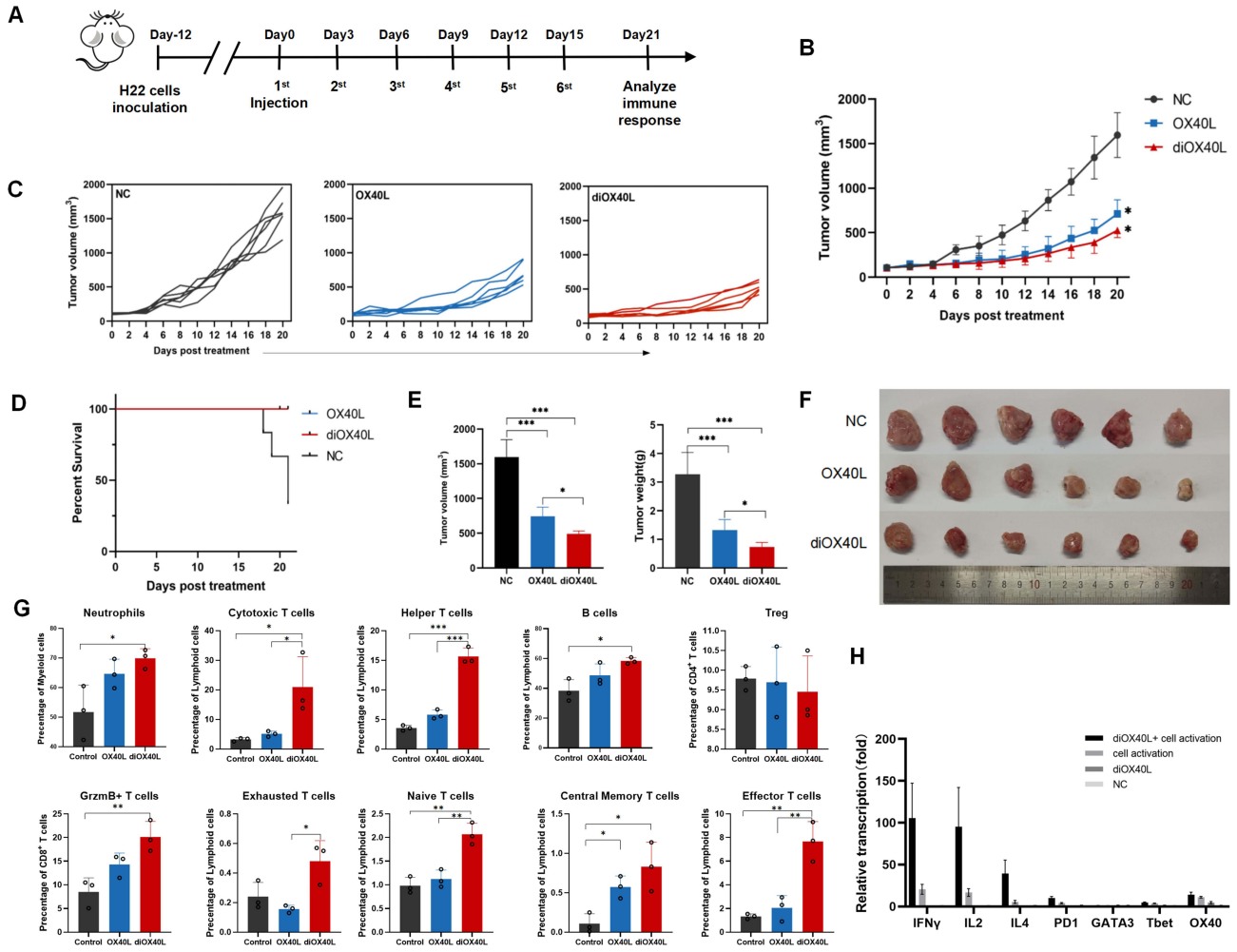

Figure 3 The optimized diOX40L mRNA play a stronger role than the original sequence in inhibiting H22 subcutaneous tumors growth in vivo.FIGURE 5: **(A)** Schematic illustration of the experiment schedule.**(B)** Growth curves of subcutaneous tumors in each mouse (n = 6). **(C)** Tumor growth curves of each group. **(D)** Survival curve (n = 6). **(E)** Average tumor weight and volume of each group. **(F)** Photography of isolated tumors from each group. **(G)** Activation of immune cells detected by flow cytometry. **(H)** Transcription level detected by qPCR after co-culture of immune cells with diOX40L-treated Hep3B. Data of (**B, E, G, H**) were processed using GraphPad Prism 8 and are presented as the mean ± SD. The *P* values were analyzed by One-way ANOVA with multiple comparisons. *, $P < 0.1$; **, $P < 0.01$; ***, $P < 0.001$.

experiment results, we conducted an in vitro validation experiment using human-derived Hep3B cells and T cells. In addition, real-time quantitative PCR was performed to evaluate the levels of IFNγ, IL-2, IL-4, PD1, OX40, Gata3 and Tbet by coculture T cells and Hep3B cells transfected diOX40L. The results of qPCR showed that the levels of IFNγ, IL-2, IL-4, PD1 and OX40 in PBMC were significantly increased in diOX40L group, which indicated that the mechanisms of diOX40L may play an antitumor effect by regulating the secretion of IFNγ, IL-2 and IL-4. Meanwhile, the expression of OX40 (the receptor of OX40L) and PD1 was also increased. This indicates that in addition to the OX40 receptor, the PD1-PDL1 pathway also plays a role (Figure 3H). In summary, these results suggested that intratumoral injection of diOX40L in mice can exert an antitumor effect, which may be achieved by regulating the phenotypes of immune cells or the secretion of cytokines in the tumor microenvironment.

For Tumors Sensitive to ICIs, Activation of TIME Can Enhance Its Antitumor Effect

To investigate whether the in vivo mRNA-translated diOX40L possess the potential of adjuvant immune checkpoint inhibitors, we assessed the therapeutic effect of the diOX40L agent in combination with the anti-PD1 antibody (aPD-1) against H22 tumors. The diOX40L agent was intratumorally administrated once every three days as before and systemic intraperitoneal (i.p.) aPD-1 was administration twice a week (Figure 4A). When the tumor volume exceeded 1500 mm^3,

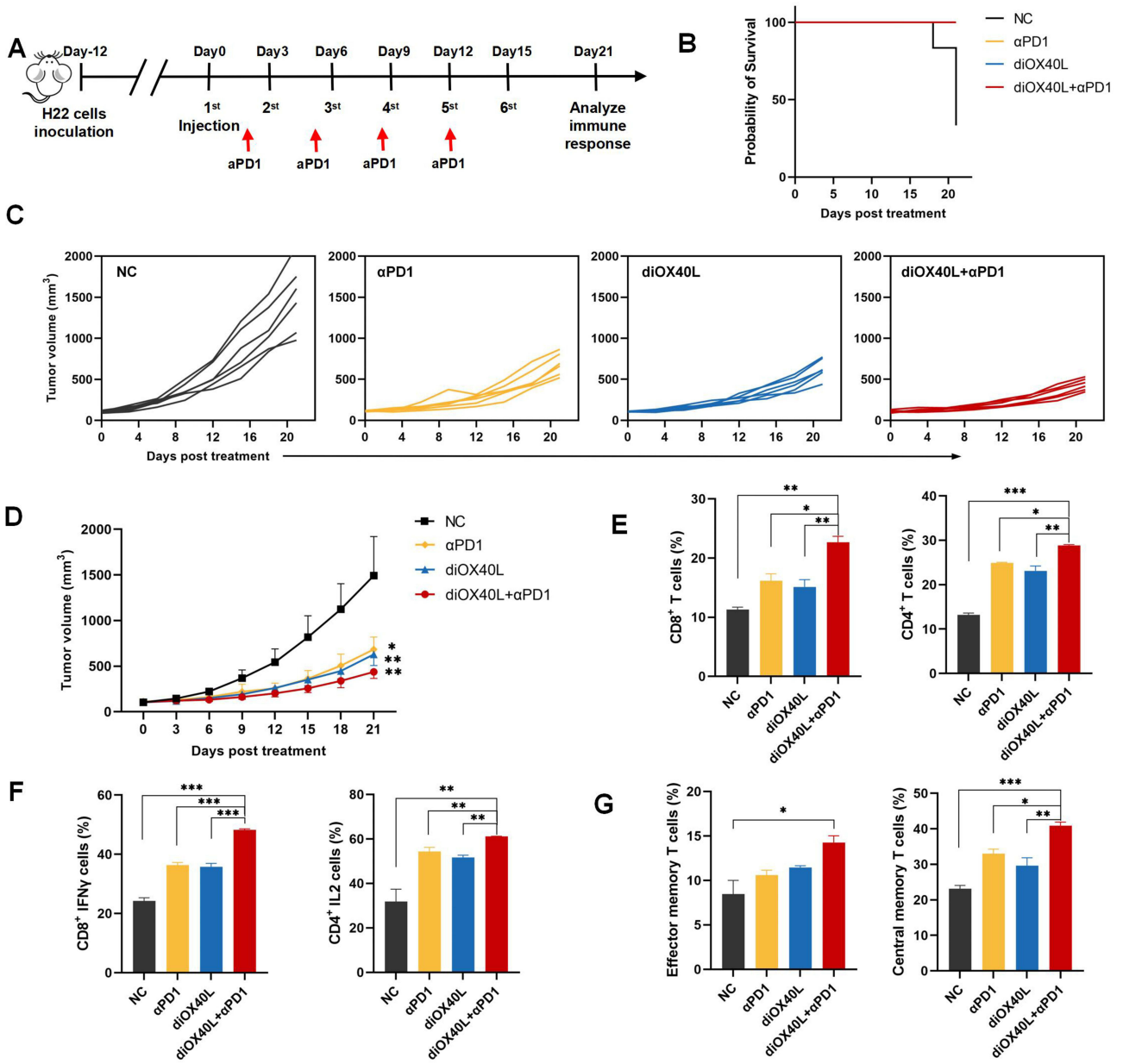

Figure 4 Improved antitumor efficacy with combination of diOX40L mRNA therapy and checkpoint blockade. (**A**) Schematic illustration of the experiment schedule with anti–PD-1. (**B**) Survival curves of H22 tumor-bearing mice after treatment with a single diOX40L mRNA intratumorally with or without anti–PD-1. (**C**) Growth curves of subcutaneous tumors in each mouse (n = 6). (**D**) Tumor growth curves of each group. (**E**) T-cell activation by flow cytometry. $CD4^+$ T cells and $CD8^+$ T cells in the tumors of the H22 tumor-bearing BALB/c mice. (**F**) Quantification of IFNγ expression in $CD8^+$ T cells and IL2 expression in $CD4^+$ T cells. (**G**) Quantification of two types of memory T cells from tumors. Statistical analyses were performed by one-way ANOVA with *P* values corrected for multiple comparisons. *, $P < 0.1$; **, $P < 0.01$; ***, $P < 0.001$. Data were presented as mean values ± SD.

the animal was considered dead. Without any intervention, the probability of survival was less than 50% by 21 days (Figure 4B). The recordings of tumor volume showed that the combination strategy was significantly more effective than any of it given alone in inhibiting the progression of H22 tumors in vivo (Figure 4C-D). A third of the subcutaneous H22 tumors were declined after the combined treatment with diOX40L and aPD-1. We can see that H22 tumors are sensitive to immune checkpoint inhibitors (Figure 4C-D). Therefore, for cancers that are susceptible to ICIs, the effective of ICIs on tumors can be enhanced by stimulating the tumor microenvironment. We then performed the immune cell analysis of the tumor tissue using flow cytometry. It is generally known that aPD-1 primarily target T cells in order to counteract tumors tendency to escape the immune system in the tumor microenvironment. So the detection and analysis of flow

https://doi.org/10.2147/IJN.S479434

cytometry mainly focused on T cells. Combination therapy significantly increased the proportion of $CD4^+$ and $CD8^+$ T cells in lymphocytes in the TEM compared to the control groups (Figure 4E). By T cell activation assays, up to 45% of $CD8^+$ T cells secreted IFNγ and up to 60% of $CD4^+$ T cells secreted IL2 in the TIEM in the combined therapy group, which were much higher than those in the control group (Figure 4F). We analyzed that the combination treatment increased the proportion of both central memory T cells ($CD44^+$ $CD62L^+$) and effector memory T cells ($CD44^+$ $CD62L^-$) in the tumor tissues (Figure 4G). The results demonstrated that diOX40L can activate the tumor immune microenvironment, enhance the memory immune effect of T cells on tumor antigens, and combination with aPD-1 is superior to any single dose alone in improving immune efficacy.

Antitumor Effect Exerted by the diOX40L mRNA in the B16F10 Melanoma Mouse Model

To further evaluate the therapeutic potential of OX40L mediated T cell costimulation in various sensitivity tumor models, B16F10 melanoma models were constructed to examine the sensitivity to t diOX40L mRNA agent combined with aPD-1. Due to the high malignancy of melanoma, we intratumorally administered the mRNA preparations once a day and give systemic intraperitoneal injections of aPD-1 twice a week (Figure 5A). The combined treatment group had the smallest

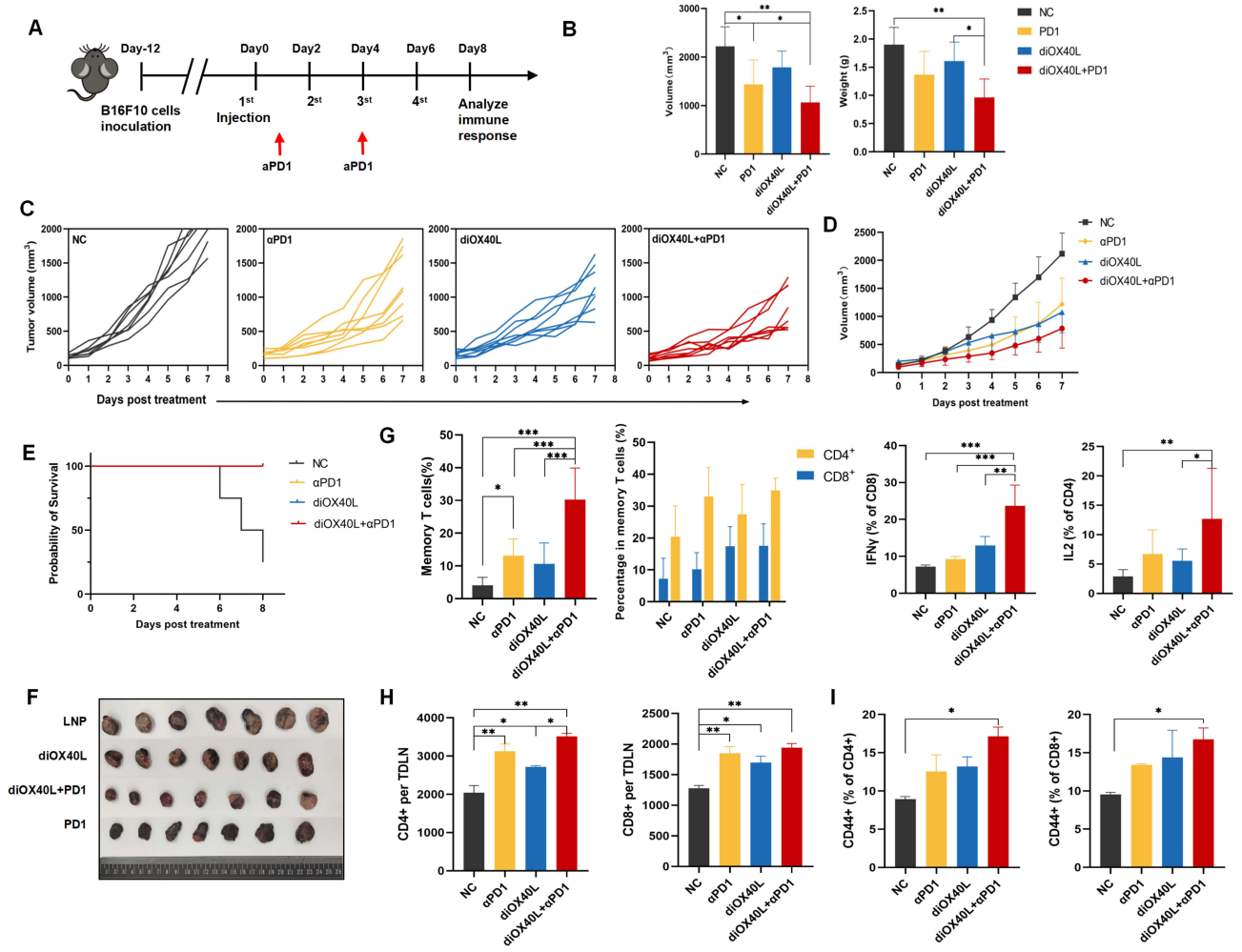

Figure 5 The diOX40L mRNA agent increase the therapeutic efficacy in multiple tumor models. **(A)** Schematic illustration of the experiment schedule in the B16F10 tumor-bearing mouse model. **(B)** Average tumor volume and weight of each group. **(C)** Growth curves of subcutaneous tumors in each mouse (n = 8). **(D)** Tumor growth curves of each group. **(E)** Survival curve (n=8). **(F)** Photography of isolated tumors from each group. **(G)** Quantification of tumor infiltrating $CD4^+$ T cells, $CD8^+$ T cells, $IFN\gamma^+$ T cells and IL-2^+ T cells in each group. **(H)** Quantification of $CD4^+$ T cells and $CD8^+$ T cells of per TdLN in each group. **(I)** Frequency of $CD44^+$ T cells in $CD4^+$ T cells and $CD8^+$ T cells, respectively. Statistical analyses were performed by one-way ANOVA with *P* values corrected for multiple comparisons. *, $P < 0.1$; **, $P < 0.01$; ***, $P < 0.001$. Data were presented as mean values ± SD.

tumor volume and weight, as illustrated in Figure 5B. By monitoring tumor volumes in mice, we can see that the inhibitory effect of the aPD-1 on B16F10 tumors was gradually diminished and three-eighth of the mice developed resistance to aPD-1 at later stages (Figure 5C). Administration of diOX40L mRNA agent showed an antitumor enhancement in aPD-1 tolerant melanoma (Figure 5D). In contrast to the NC group, 75% of survival were rescued through experimental dosing after 20 days upon challenge with B16F10 cells (Figure 5E). The photography of isolated tumors from each group on day 7 is shown on Figure 5F. These findings suggest that aPD-1 combined with diOX40L mRNA agents could lessen tumor cells' resistance towards aPD-1 and elicit potent antitumor effects that with an unfavorable TME.

DiOX40L mRNA Agent Promotes Immune Activation and TME Remodeling

Since we observed an increase in types of memory T cells in the H22 antitumor model, similar analysis of melanoma demonstrated that memory T cells were similarly increased in the TIME after the combination therapy, and the majority were $CD4^+$ T cells (Figure 5G). These T cells secrete both IL 2 and IFNγ. When we isolated and examined tumor-draining lymph nodes (TDLN) in melanoma, both $CD4^+$ and $CD8^+$ T cells in the TDLNs were relatively abundant in the experimental groups (Figure 5H). The memory cells in the TDLNs showed an activated state ($CD69^+CD44^+$) in Figure 5I. From this, we speculated that the effector T cells in the tumor microenvironment arise from migration of the TDLNs. The mRNA-translated diOX40L as an up-regulated T cells adaptor reconstructed the immune tolerance state by increasing memory T cells in the TEM. Even for melanoma, an immune ICI-resistant tumor, the combination of diOX40L agents and systemic intraperitoneal administration of aPD-1 is a promising therapeutic approach. Finally, the Hematoxylin and Eosin (HE) staining in different organs showed no abnormalities after treatment with different regimens (Figure 6A). Whether there was any irreversible liver or renal impairment was indicated by serum alanine transaminase (ALT), aspartate transaminase (AST), and creatine kinase (CK) levels. The results showed that although the data of the experimental groups were slightly higher than those of the negative control group, there was no statistical difference between the groups (Figure 6B–D).

Discussion

In the realm of cancer treatment, immune checkpoint inhibitors have displayed remarkable potential as an emerging form of immunotherapy. Nevertheless, the formidable hurdle of tumor-induced immune suppression has remained a substantial barrier to effective cancer immunotherapy.[8] Recently, increasing numbers of immune targets have been developed to reverse the refractory TIME.[28] The OX40-OX40L axis is typically used in cancer immunotherapy to co-stimulate the immune system and to eradicate tumors through adjuvant immunotherapy.[29–32] This strategy could be achieved mainly by increasing the activity of OX40 on T cells. The major forms of existing treatment are agonist OX40 antibodies and gene therapies that mimic OX40L to improve connection to OX40.[18] Gene therapy incorporating OX40L expression has gained prominence recently, driven by the shortcomings of protein-based medicines, such as their time-consuming production, persisting impurities, and tendency to aggregate.[27,33–35] In this study, mRNA encoding sequences were adopted to express the OX40L protein. Because the mRNA therapy stands out as a safer alternative to other forms of gene therapy, as it does not require entry into the cell nucleus and does not integrate into the genome.[36] This quality makes it an appealing option for cancer immunotherapy, holding significant promise in the battle against cancer. Presently, patients with diverse cancer diagnoses are actively participating in numerous clinical trials to assess the efficacy of mRNA agents in treatment.[37]

The rationale for using mRNA agents for immunotherapy is to use mRNA-encoded proteins to modify the tumor microenvironment.[38,39] In this study, we have presented a significant exploration of diOX40L mRNA preparation and its impact on modulating the tumor microenvironment and counteracting tumor immunosuppression. The application of this method is limited by the screening mRNA structures and delivery techniques. To address the aforementioned challenges, researchers employ continuous sequence optimization through bioinformatics techniques tailored to the specific requirements of developing various types of drugs.[40,41] We have similarly taken these approaches. OX40L is expressed in trimeric form and binds three OX40 molecules with high affinity and slow dissociation, which is a crucial characteristic for its role in immunomodulation.[42,43] To more effectively enhance the interaction of the OX40 to OX40L, a series of

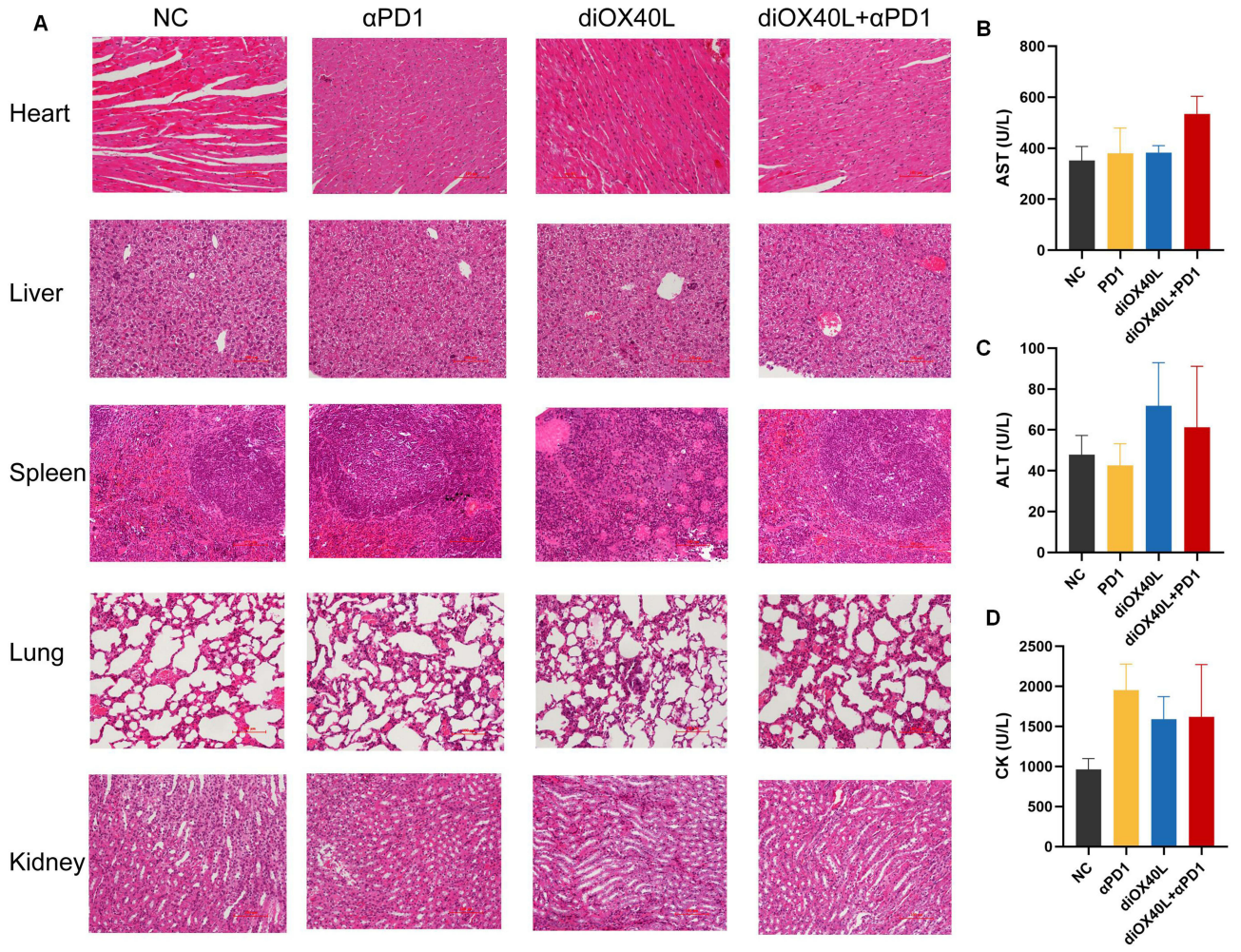

Figure 6 Safety and Toxicity Evaluation. (**A**) The HE staining of the different organs from mice after treatment with different regimens. Scale bar = 100 μm. (**B**) Serum AST Level. (**C**) Serum ALT Level. (**D**) Serum CK Level. Statistical analyses were performed by one-way ANOVA.

optimization strategies were implemented. The OX40L sequence was optimized, and the double OX40L sequence was linked together in the opening reading frame. The increase of Kozak sequence can regulate the initiation of translation, and this ensured that the protein synthesis process was more efficient and accurately controlled. Meanwhile, the use of N1 methyl-modified UTP favors stabilizing mRNA, thereby reducing its immunogenicity.[44,45] Our optimized sequence demonstrated increased OX40L production both in vitro and in vivo, which was a crucial starting point.

Additionally, two of the more commonly employed delivery systems for mRNA are LNP and lipoplex (LPX).[46,47] LNP is currently considered the most ideal delivery system, consisting of neutral lipid, cationic liposome, cholesterol, and PEG-lipid.[48] The mRNA is a typical technology platform, with its standard operation process and strong scalability.[49] Ideally, all components can be pre-prepared, except for the encoding area. With the support of well-established LNP delivery technology, mRNA can rapidly expand its applications into various areas of tumor immunity research.[50] So after the diOX40L-mRNA was synthesized through in vitro transcription, capping, and tail addition procedures, it was uniformly coated around LNP by advanced microfluidic technology.[51] Subsequently, the diOX40L mRNA agents were finally obtained through a purification process to remove impurities, ensuring the purity and quality of the final product.

This study primarily showcases the capacity of diOX40L mRNA preparation to modulate the tumor microenvironment and counteract tumor immunosuppression in vivo. The comparative analysis between the optimized and original sequences in H22 subcutaneous tumor-bearing mice revealed the superior antitumor effects of the optimized diOX40L

mRNA agents, as evidenced by cytotoxic T cell activation, tumor volume reduction, and overall survival. By co-culturing T cells with Hep3B cells transfected with the mRNA agents in vitro, it was found that in addition to the OX40-OX40L axis playing a role, the PD1-PDL1 axis may also play a role. This is similar to previous studies.[29,52,53] We then proceeded to combine the diOX40L mRNA agents with aPD1 therapy to assess the feasibility of adjuvant immunotherapy. The results were highly promising, especially in tumors sensitive to immunotherapy. This approach not only activated T cells but also increased central memory cells and effector memory T cells within the TME. To further investigate the origins of these memory cells and the broad efficacy of diOX40L mRNA agents, we extended our combination strategy with aPD1 to a B16F10 melanoma model. Melanoma, with its high malignancy and resistance to ICIs, required us to identify novel combinations integrating ICIs with different agents for clinical treatment guidance.[54–56] The results found that intratumoral injection of diOX40L mRNA preparations combined with intraperitoneal administration of aPD1 led to a remarkable delay in tumor development compared to any single-dose group. This transformed the 'cold' immune-evasive TME into a 'hot' state, facilitating tumor cell elimination.[57] This was achieved through the migration of memory cells from the TDLNs, activation of T cells within the TME, and the release of cytokines. In conclusion, experimental results demonstrated that local delivery of diOX40L mRNA yielded several significant outcomes: (1) direct increase of the cytotoxic effects of T cells; (2) increased T cell infiltration and the activation of the TIME; (3) adjuvant killing of H22 tumors sensitive to aPD1; (4) broad-spectrum antitumor effects to the B16F10 melanoma mouse model; (5) increased infiltration of central memory T cells and effector T cells; (6) migration of memory cells from the TDLNs.

Conclusion

The OX40-OX40L axis emerges as one of the most vital costimulatory molecular axes for regulating T cells. Our findings confirm its potential to enhance various types of T cells and impede the progression of malignancies. Importantly, this study provides a theoretical foundation for clinical treatments, showing that OX40 activation can complement T cell checkpoint blockade like aPD1 and reshape the refractory TME. Future research will focus on validating this agent in more experimental animals and other tumors. Additionally, we will explore its potential in clinical applications.

Acknowledgment

The authors would like to thank the professor at Institute of Biophysics, Chinese Academy of Science, Pengyuan Yang for his assistance in carrying out the immunity study. In particular, the authors would like to thank Yanan Gao for her carrying out the flow cytometry investigation.

Disclosure

The authors report no conflicts of interest in this work.

References

1. Yang JD, Hainaut P, Gores GJ, Amadou A, Plymoth A, Roberts LR. A global view of hepatocellular carcinoma: trends, risk, prevention and management. *Nat Rev Gastroenterol Hepatol*. 2019;16(10):589–604. doi:10.1038/s41575-019-0186-y
2. Cabibbo G, Enea M, Attanasio M, Bruix J, Craxi A, Camma C. A meta-analysis of survival rates of untreated patients in randomized clinical trials of hepatocellular carcinoma. *Hepatology*. 2010;51(4):1274–1283. doi:10.1002/hep.23485
3. Bruni D, Angell HK, Galon J. The immune contexture and Immunoscore in cancer prognosis and therapeutic efficacy. *Nat Rev Cancer*. 2020;20(11):662–680. doi:10.1038/s41568-020-0285-7
4. El-Khoueiry AB, Sangro B, Yau T, et al. Nivolumab in patients with advanced hepatocellular carcinoma (CheckMate 040): an open-label, non-comparative, Phase 1/2 dose escalation and expansion trial. *Lancet*. 2017;389(10088):2492–2502. doi:10.1016/S0140-6736(17)31046-2
5. Sharma P, Hu-Lieskovan S, Wargo JA, Ribas A. Primary, adaptive, and acquired resistance to cancer immunotherapy. *Cell*. 2017;168(4):707–723. doi:10.1016/j.cell.2017.01.017
6. Liu K, Cui JJ, Zhan Y, et al. Reprogramming the tumor microenvironment by genome editing for precision cancer therapy. *mol Cancer*. 2022;21(1):98.
7. Philip M, Fairchild L, Sun L, et al. Chromatin states define tumour-specific T cell dysfunction and reprogramming. *Nature*. 2017;545(7655):452–456. doi:10.1038/nature22367
8. Emens LA, Silverstein SC, Khleif S, Marincola FM, Galon J. Toward integrative cancer immunotherapy: targeting the tumor microenvironment. *J Transl Med*. 2012;10(1):70. doi:10.1186/1479-5876-10-70

9. Bai J, Gao Z, Li X, Dong L, Han W, Nie J. Regulation of PD-1/PD-L1 pathway and resistance to PD-1/PD-L1 blockade. *Oncotarget*. 2017;8(66):110693–110707. doi:10.18632/oncotarget.22690
10. Rizzo A. Identifying optimal first-line treatment for advanced non-small cell lung carcinoma with high PD-L1 expression: a matter of debate. *Br. J. Cancer*. 2022;127(8):1381–1382. doi:10.1038/s41416-022-01929-w
11. Rizzo A, Mollica V, Massari F. Expression of programmed cell death ligand 1 as a predictive biomarker in metastatic urothelial carcinoma patients treated with first-line immune checkpoint inhibitors versus chemotherapy: a systematic review and meta-analysis. *Eur Urology Focus*. 2022;8(1):152–159. doi:10.1016/j.euf.2021.01.003
12. Choi Y, Shi Y, Haymaker CL, Naing A, Ciliberto G, Hajjar J. T-cell agonists in cancer immunotherapy. *J Immunother Cancer*. 2020;8(2):e000966. doi:10.1136/jitc-2020-000966
13. Vonderheide RH. CD40 agonist antibodies in cancer immunotherapy. *Annu Rev Med*. 2020;71(1):47–58. doi:10.1146/annurev-med-062518-045435
14. Curti BD, Kovacsovics-Bankowski M, Morris N, et al. OX40 is a potent immune-stimulating target in late-stage cancer patients. *Cancer Res*. 2013;73(24):7189–7198. doi:10.1158/0008-5472.CAN-12-4174
15. Fu Y, Lin Q, Zhang Z, Zhang L. Therapeutic strategies for the costimulatory molecule OX40 in T-cell-mediated immunity. *Acta Pharm Sin B*. 2020;10(3):414–433. doi:10.1016/j.apsb.2019.08.010
16. Pan PY, Zang Y, Weber K, Meseck ML, Chen SH. OX40 ligation enhances primary and memory cytotoxic T lymphocyte responses in an immunotherapy for hepatic colon metastases. *Mol Ther*. 2002;6(4):528–536. doi:10.1006/mthe.2002.0699
17. Weinberg AD, Rivera MM, Prell R, et al. Engagement of the OX-40 receptor in vivo enhances antitumor immunity. *J Immunol*. 2000;164(4):2160–2169. doi:10.4049/jimmunol.164.4.2160
18. Aspeslagh S, Postel-Vinay S, Rusakiewicz S, Soria JC, Zitvogel L, Marabelle A. Rationale for anti-OX40 cancer immunotherapy. *Eur J Cancer*. 2016;52:50–66. doi:10.1016/j.ejca.2015.08.021
19. Croft M. Control of immunity by the TNFR-related molecule OX40 (CD134). *Annu Rev Immunol*. 2010;28(1):57–78. doi:10.1146/annurev-immunol-030409-101243
20. Goswami S, Wang W, Arakawa T, Ohtake S. Developments and Challenges for mAb-Based Therapeutics. *Antibodies*. 2013;2(4):452–500.
21. Miao L, Zhang Y, Huang L. mRNA vaccine for cancer immunotherapy. *mol Cancer*. 2021;20(1):41. doi:10.1186/s12943-021-01335-5
22. Deng Z, Tian Y, Song J, An G, Yang P. mRNA Vaccines: the Dawn of a New Era of Cancer Immunotherapy. *Front Immunol*. 2022;13:887125. doi:10.3389/fimmu.2022.887125
23. Jimeno A, Gupta S, Sullivan R, et al. A phase 1/2, open-label, multicenter, dose escalation and efficacy study of mRNA-2416, a lipid nanoparticle encapsulated mRNA encoding human OX40L, for intratumoral injection alone or in combination with durvalumab for patients with advanced malignancies. *Cancer Res*. 2020;80(16):CT032–CT032. doi:10.1158/1538-7445.AM2020-CT032
24. Bauer T, Patel M, Jimeno A, et al. Abstract CT210: a Phase I, open-label, multicenter, dose escalation study of mRNA-2752, a lipid nanoparticle encapsulating mRNAs encoding human OX40L, IL-23, and IL-36γ, for intratumoral injection alone and in combination with immune checkpoint blockade. *Cancer Res*. 2019;79(13_Supplement):CT210–CT210. doi:10.1158/1538-7445.AM2019-CT210
25. Patel MR, Bauer TM, Jimeno A, et al. A phase I study of mRNA-2752, a lipid nanoparticle encapsulating mRNAs encoding human OX40L, IL-23, and IL-36 gamma, for intratumoral (iTu) injection alone and in combination with durvalumab. *J Clin Oncol*. 2020;38(15).
26. Deng Z, Yang H, Tian Y, Liu Z, Sun F, Yang P. An OX40L mRNA vaccine inhibits the growth of hepatocellular carcinoma. *Front Oncol*. 2022;12:975408. doi:10.3389/fonc.2022.975408
27. Hewitt SL, Bai A, Bailey D, et al. Durable anticancer immunity from intratumoral administration of IL-23, IL-36gamma, and OX40L mRNAs. *Sci Transl Med*. 2019;11(477). doi:10.1126/scitranslmed.aat9143.
28. Arens R, Scheeren FA. Genetic screening for novel regulators of immune checkpoint molecules. *Trends Immunol*. 2020;41(8):692–705. doi:10.1016/j.it.2020.06.005
29. Polesso F, Weinberg AD, Moran AE. Late-stage tumor regression after PD-L1 blockade plus a concurrent OX40 agonist. *Cancer Immunol Res*. 2019;7(2):269–281. doi:10.1158/2326-6066.CIR-18-0222
30. Redmond WL, Linch SN, Kasiewicz MJ. Combined targeting of costimulatory (OX40) and coinhibitory (CTLA-4) pathways elicits potent effector T cells capable of driving robust antitumor immunity. *Cancer Immunol Res*. 2014;2(2):142–153. doi:10.1158/2326-6066.CIR-13-0031-T
31. Yadav R, Redmond WL. Current Clinical Trial Landscape of OX40 Agonists. *Curr Oncol Rep*. 2022;24(7):951–960. doi:10.1007/s11912-022-01265-5
32. Linch SN, McNamara MJ, Redmond WL. OX40 agonists and combination immunotherapy: putting the pedal to the metal. *Front Oncol*. 2015;5:34. doi:10.3389/fonc.2015.00034
33. Kimura T, Fukushima S, Okada E, et al. Induced pluripotent stem cell-derived myeloid cells expressing OX40 ligand amplify antigen-specific T cells in advanced melanoma. *Pigm Cell Melanoma Res*. 2020;33(5):744–755. doi:10.1111/pcmr.12887
34. Assudani DP, Ahmad M, Li G, Rees RC, Ali SA. Immunotherapeutic potential of DISC-HSV and OX40L in cancer. *Cancer Immunol, Immunotherapy: CII*. 2006;55(1):104–111. doi:10.1007/s00262-005-0004-y
35. Tian L, Liu T, Jiang S, et al. Oncolytic Newcastle disease virus expressing the co-stimulator OX40L as immunopotentiator for colorectal cancer therapy. *Gene Ther*. 2021;30(1–2):64–74. doi:10.1038/s41434-021-00256-8
36. Pardi N, Hogan MJ, Porter FW, Weissman D. mRNA vaccines - a new era in vaccinology. *Nat Rev Drug Discov*. 2018;17(4):261–279. doi:10.1038/nrd.2017.243
37. Lorentzen CL, Haanen JB, Met O, Svane IM. Clinical advances and ongoing trials on mRNA vaccines for cancer treatment. *Lancet Oncol*. 2022;23(10):e450–e458. doi:10.1016/S1470-2045(22)00372-2
38. Li X, Ma S, Gao T, Mai Y, Song Z, Yang J. The main battlefield of mRNA vaccine - Tumor immune microenvironment. *Int Immunopharmacol*. 2022;113(Pt A):109367. doi:10.1016/j.intimp.2022.109367
39. Hewitt SL, Bailey D, Zielinski J, et al. Intratumoral IL12 mRNA therapy promotes TH1 transformation of the tumor microenvironment. *Clin Cancer Res*. 2020;26(23):6284–6298. doi:10.1158/1078-0432.CCR-20-0472
40. Zhang H, Zhang L, Lin A, et al. Algorithm for optimized mRNA design improves stability and immunogenicity. *Nature*. 2023;621(7978):396–403.
41. Rice AM, Castillo Morales A, Ho AT, et al. Evidence for strong mutation bias toward, and selection against, U content in SARS-CoV-2: implications for vaccine design. *mol Biol Evolution*. 2021;38(1):67–83. doi:10.1093/molbev/msaa188

42. Croft M, So T, Duan W, Soroosh P. The significance of OX40 and OX40L to T-cell biology and immune disease. *Immunol Rev*. 2009;229 (1):173–191. doi:10.1111/j.1600-065X.2009.00766.x
43. Pippig SD, Pena-Rossi C, Long J, et al. Robust B cell immunity but impaired T cell proliferation in the absence of CD134 (OX40). *J Immunol*. 1999;163(12):6520–6529. doi:10.4049/jimmunol.163.12.6520
44. Svitkin YV, Cheng YM, Chakraborty T, Presnyak V, John M, Sonenberg N. N1-methyl-pseudouridine in mRNA enhances translation through eIF2alpha-dependent and independent mechanisms by increasing ribosome density. *Nucleic Acids Res*. 2017;45(10):6023–6036. doi:10.1093/nar/gkx135
45. Acevedo JM, Hoermann B, Schlimbach T, Teleman AA. Changes in global translation elongation or initiation rates shape the proteome via the Kozak sequence. *Sci Rep*. 2018;8(1):4018. doi:10.1038/s41598-018-22330-9
46. Reinhard K, Rengstl B, Oehm P, et al. An RNA vaccine drives expansion and efficacy of claudin-CAR-T cells against solid tumors. *Science*. 2020;367(6476):446–453. doi:10.1126/science.aay5967
47. Sahin U, Oehm P, Derhovanessian E, et al. An RNA vaccine drives immunity in checkpoint-inhibitor-treated melanoma. *Nature*. 2020;585 (7823):107–112. doi:10.1038/s41586-020-2537-9
48. Zhang Y, Sun C, Wang C, Jankovic KE, Dong Y. Lipids and Lipid Derivatives for RNA Delivery. *Chem Rev*. 2021;121(20):12181–12277. doi:10.1021/acs.chemrev.1c00244
49. Hou X, Zaks T, Langer R, Dong Y. Lipid nanoparticles for mRNA delivery. *Nat Rev Mater*. 2021;6(12):1078–1094. doi:10.1038/s41578-021-00358-0
50. Wang C, Zhang Y, Dong Y. Lipid Nanoparticle-mRNA formulations for therapeutic applications. *Acc Chem Res*. 2021;54(23):4283–4293. doi:10.1021/acs.accounts.1c00550
51. Maeki M, Uno S, Niwa A, Okada Y, Tokeshi M. Microfluidic technologies and devices for lipid nanoparticle-based RNA delivery. *J Control Release*. 2022;344:80–96. doi:10.1016/j.jconrel.2022.02.017
52. Kuang Z, Pu P, Wu M, et al. A Novel Bispecific Antibody with PD-L1-assisted OX40 Activation for Cancer Treatment. *mol Cancer Ther*. 2020;19 (12):2564–2574. doi:10.1158/1535-7163.MCT-20-0226
53. Kraehenbuehl L, Weng CH, Eghbali S, Wolchok JD, Merghoub T. Enhancing immunotherapy in cancer by targeting emerging immunomodulatory pathways. *Nat Rev Clin Oncol*. 2022;19(1):37–50. doi:10.1038/s41571-021-00552-7
54. Leong A, Kim M. The Angiopoietin-2 and TIE pathway as a therapeutic target for enhancing antiangiogenic therapy and immunotherapy in patients with advanced cancer. *Int J mol Sci*. 2020;21(22):8689. doi:10.3390/ijms21228689
55. Larkin J, Chiarion-Sileni V, Gonzalez R, et al. Combined nivolumab and ipilimumab or monotherapy in untreated melanoma. *New Engl J Med*. 2015;373(1):23–34. doi:10.1056/NEJMoa1504030
56. Postow MA, Chesney J, Pavlick AC, et al. Nivolumab and ipilimumab versus ipilimumab in untreated melanoma. *New Engl J Med*. 2015;372 (21):2006–2017. doi:10.1056/NEJMoa1414428
57. Rostamizadeh L, Molavi O, Rashid M, et al. Recent advances in cancer immunotherapy: modulation of tumor microenvironment by Toll-like receptor ligands. *BioImpacts: BI*. 2022;12(3):261–290. doi:10.34172/bi.2022.23896

International Journal of Nanomedicine

Dovepress
Taylor & Francis Group

Publish your work in this journal

The International Journal of Nanomedicine is an international, peer-reviewed journal focusing on the application of nanotechnology in diagnostics, therapeutics, and drug delivery systems throughout the biomedical field. This journal is indexed on PubMed Central, MedLine, CAS, SciSearch®, Current Contents®/Clinical Medicine, Journal Citation Reports/Science Edition, EMBase, Scopus and the Elsevier Bibliographic databases. The manuscript management system is completely online and includes a very quick and fair peer-review system, which is all easy to use. Visit http://www.dovepress.com/testimonials.php to read real quotes from published authors.

Submit your manuscript here: https://www.dovepress.com/international-journal-of-nanomedicine-journal